Phase average velocity field in the vicinity of an isolated wheel model

Laurent-Emmanuel BRIZZI[(1)] - Alain NOEL[(2)] - Vincent HERBERT[(2)]
[(1)] Laboratoire d'Etudes Aérodynamiques, Université de Poitiers, SP2MI, Boulevard Pierre et Marie CURIE, Téléport 2, BP 30179, 86960 FUTUROSCOPE CHASSENEUIL CEDEX, France
Tél : (33) 05 49 49 69 27
FAX : (33) 05 49 49 69 68
e-mail : Laurent.brizzi@lea.univ-poitiers.fr

[(2)] PSA Peugeot Citroën, Direction de la Recherche et de l'Innovation Automobile, 2 route de Gisy, 78943 Velizy-Villacoublay

Abstract

During the past five years, the Laboratoire d'Etude Aérodynamique (LEA) of Poitiers University collaborates with PSA (car manufacturer) on several studies concerning aerodynamic and thermal problems (Noel (2001)). One of these studies deals with the characterization of the flow field (Pressure, Velocity and Temperature) in and around a car wheel model. One of the aims is to validate numerical tools to correctly predict the heat transfer in the vicinity of the brakes. These measurements (Pressure, Velocity and Temperature) are realized both inside and outside an isolated car wheel model. The main analyzed parameters are the main flow velocity, the wheel angular velocity and the geometry of the rim holes.

In this paper, we report an experimental investigation on the flow field in the vicinity of an isolated simplified wheel (2/5 scale model) rotating in an open wind tunnel. The components of the model wheel are reduced to the drive shaft, the brake disc and the tire-rim system. Visualizations, non-intrusive experimental techniques (LDV and PIV) and pressure measurement have been used to measure the aerodynamic flow fields, both around the wheel and through the rim holes.

During this study, the internal and external aerodynamic of the openwork wheel is studied and then analyzed. We have thus identified the Inward/outward fluid zones near the interfaces located on the side of the wheel axle and near the holes. We observe that the fluid enters primarily on the wheel axle side and comes out on the side holes and downstream of the wheel axle. The separation areas present on the upstream parts of each face of the wheel play a fundamental role in the fluid transfers between the inside and the outside of the whell. The fluid entrance on the wheel axle side is due to the separation closure whereas the fluid exit by the holes is due to the presence of the reverse flow zone on the openwork face and coupling with the fluid deceleration during its reattachment.

In addition, measurements were also carried out by PIV in this plan when the wheel is in rotation. They reveal that the fluid comes out of the wheel at the same place. However, the exit fluid velocities are lower and the disturbance of the separation area is less because of the distribution effect of the outgoing fluid by the holes. This distribution causes a drop of the local exit velocities. Measurements, using "conditional" PIV, consist of finding the location of the wheel position during the acquisition are then carried out. The processing of these measurements allows us to observe a periodic fluid expulsion each time that an opening crosses the plan of measurement.

In conclusion, the analysis of theses experimental investigations give interesting insights on the flow organization in the vicinity of the wheel which can be useful to understand the heat transfer of a wheel brake disc.

The significant contribution of the wheels to the total Cx of the cars justifies the study of their external aerodynamics. Indeed, Wickern *et al.* (1997) indicates that the drag related to the wheels represents 25 % of the total drag. Most of the previous studies concern wheels assembled on vehicle and around the isolated wheels. In this paper we will limit our presentation to the flow around an isolated wheel even if there are similarities between the flow around the isolated wheels and of the wheels assembled on vehicle.

There are only few authors who carry out a detailed description of the flow around a wheel (Fackrell and Harvey (1973) and (1974), Cogotti (1983) and (1991), Mercker et al.(1992) and (1992), Stapelford and Carr (1997) and Axon et al (1998)) . The low number of studies present in the literature is related to the fact that the experimental set-up is usually complex to realize.

In this paper, we report an experimental investigation on the flow field in the vicinity of an isolated simplified wheel (2/5 scale model) rotating in an open wind tunnel. Visualizations, non-intrusive experimental techniques (LDV and PIV) and pressure measurement have been used to measure the aerodynamic flow fields, both around the wheel and through the rim holes in order to identify the exchanges through the interfaces.

Experimental Device

The experiments were carried out at the Laboratoire d'Etudes Aérodynamiques of Poitiers University. The experimental work was performed in an Eiffel type wind tunnel (open circuit, cf. Figure 1) having a transparent (glass) working section that is 400 mm high, 300 mm wide and 1300 mm long. The convergent is preceded by a filter, a honeycomb (30 mm wide and 60 mm long cells) and a fine grid (5 mm) located 420 mm upstream of the test chamber entrance in order to provide a uniform flow. A turbulent boundary layer was created using a strip of sandpaper (38 mm wide and spanning the whole width of the tunnel, grain size of 310 µm) which was placed at the bottom entrance of the test chamber. A Pitot tube and a type K thermocouple were used to control the free-stream velocity of the tunnel and to check the temperature at the entrance. The velocity profile was measured with a single hot wire anemometer at 400 mm from the entrance and obeyed a power-law equation.

For a real car wheel, we can observe that the brake disk, surrounded with the rim and the tire, is located near the shock-absorber and the direction organs. The disk is then in a complex and confined geometry. In order to simplify this complex geometry we have undertaken several simplifications. Then we have suppressed the brake pads, the brake clamp, the shock-absorber, the Cardan shaft, the bearing and the direction organs. Figure 2 shows the resulting simplified geometry where the measurements will be carried out. Simplified models are only constituted by an axis, a wheel (including the rim and the tire) and a disk. The disk side in front of the wheel axle will be called "internal side". The "external face" corresponds to the face in front of rim holes. The part of the geometry included between the disk external face and the rim holes is called "bowl". This model corresponds to wheels reduced to 2/5 scale. This scale is the best compromise between a reasonable blocking rate (≈13.6%) and a sufficient size to undertake measurements in good conditions

Our models are put in rotation inside the wind tunnel with an external rotation device. This driving system is a power lathe: the mandrel holds the wheel axle. This axis is located 600 mm downstream the inlet of the test section. The wheel is centered with respect to the lateral test section windows.

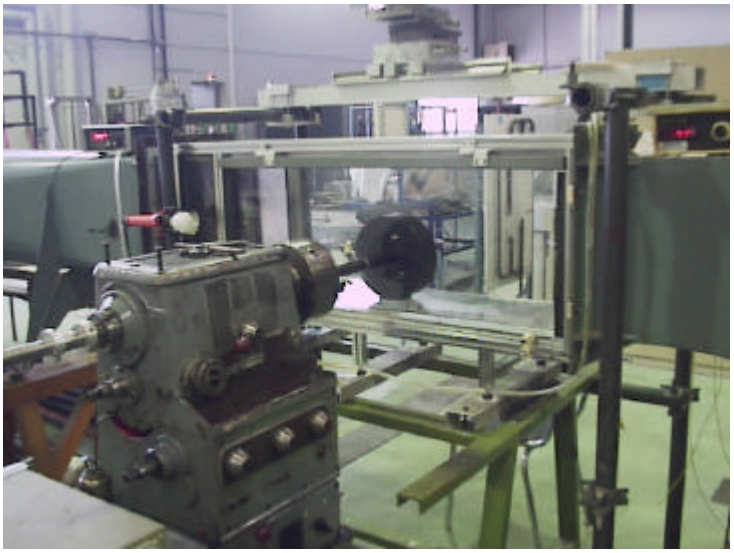

Figure 1: Driving system and wind tunnel test.

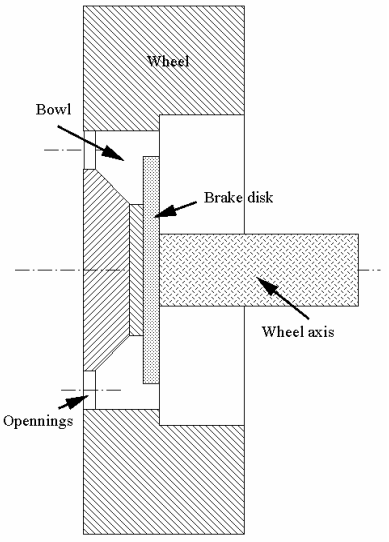

Figure 2: Simplified wheel.

In order to study the influence of the surface and the shape of the holes on the aerodynamic in the vicinity of a brake disk, three kind of wheel are tested during the experiments (cf. Figure 3). For these wheels only the dimension and the shape of the holes vary. All these wheels have the same dimensions and have the same internal volume.

The first one has the largest opening surface. The rim of this wheel, called "***open wheel***", has an opening surface divided by 12 circular holes (Figure 3a) of 17 mm diameter.

The second (a), called "***half open wheel***", has an opening surface divided by 12 circular holes (Figure 3a) of 12 mm diameter. In these conditions the total surface of the holes is divided by two.

The third one (b), called "***axisymmetric open wheel***", has the same opening surface than the "open wheel" one. But the holes shape's is different: On this wheel, a hole of 6 mm thick was milled on the rim but leaving three support legs.

In order to study the inner side of the wheel with non-intrusive techniques using LASER, it is necessary to make the wheels with a transparent tire using a PMMA (PolyMétacrylate de Méthyle) block (cf. figure 3c). For the same reason, the brake disk was also made transparent. On the other hand, for the external measurements and the pressure measurements, no particular material is needed, so we have chosen an aluminum alloy wheel. In order to minimize the flow passing under the wheel, we have added between the wheel and the floor a special element. This element is as large as the wheel, 4 mm high and 70 mm long. A piece of fitted carpet is stuck in order to ensure the sealing between the upstream and the downstream part of the wheel.

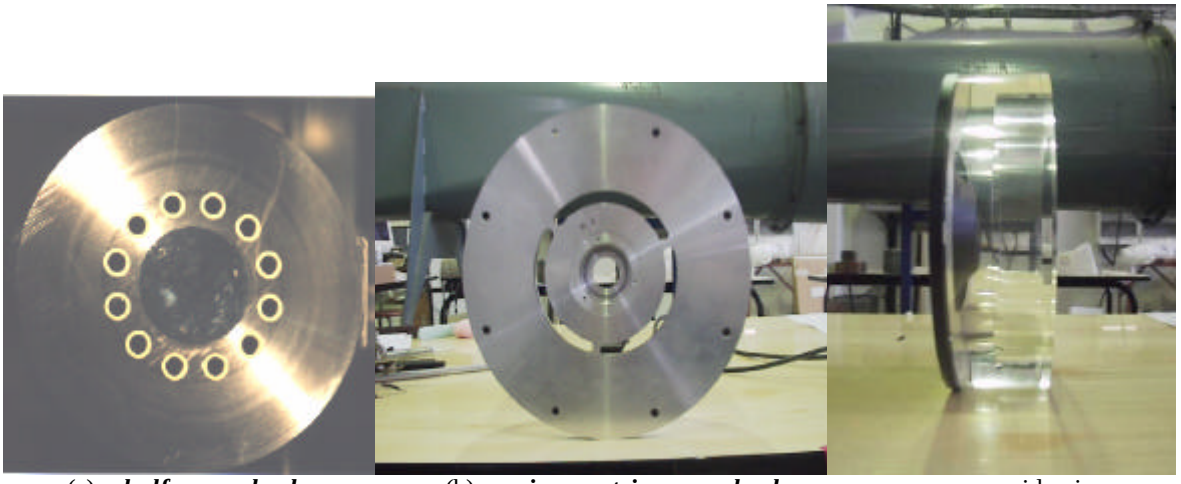

(a) « ***half open wheel*** » (b) « ***axisymmetric open wheel*** » side view

Figure 3: Rim geometries.

In this paper, the direct referential retained for the tests is defined in the following way (*cf.* Figure 4) :

- X free stream flow direction (Wind tunnel axis).
- Y vertically upward.
- Z horizontal directed toward the external part of the wheel (wheel axle).
- The origin O, intersection point between the wheel external face and the wheel axle.

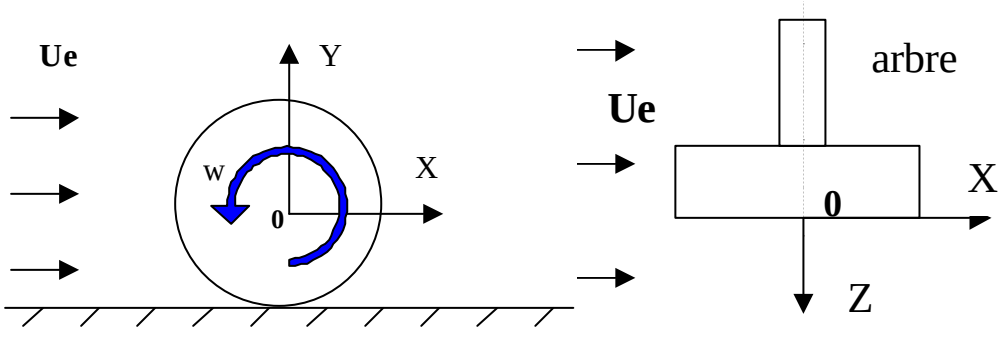

Side view *Top view*

Figure 4: Referential.

For this study, a "configuration" is the association of a rim type, a rotating velocity and a velocity of the free stream. This velocity is fixed at 13.6 m/s (49 km/h) and the rotation speed is set at 1115 rpm (corresponding

to a velocity at the wheel periphery of 13.6 m/s). Even if this velocity seems weak, previous experiments realized on real cars show that the velocity in the vicinity of the wheel is about 11 m/s for a free stream velocity of 30 m/s (108 km/h). Table 1 resumes all the studied configurations.

Configuration name	***Rim type***	***Ue (m/s)***	*w* ***(tr/min)***
B	half open wheel	13.6	1115
D	open wheel	13.6	0
F	open wheel	13.6	1115
G	axisymmetric open wheel	13.6	1115

Table 1: Studied configurations.

For this work, we focus our interest on the unsteady part of the flow field around the car wheel model and more especially near the holes. In these conditions we need the exact position of the holes during the rotation. To do this, an optical coder is fixed on the wheel axle. The coder channel, coupled with a pulse generator and a counter, resets the signal at each round in order to obtain a linear function between the wheel angle and the output (cf. figure 5).

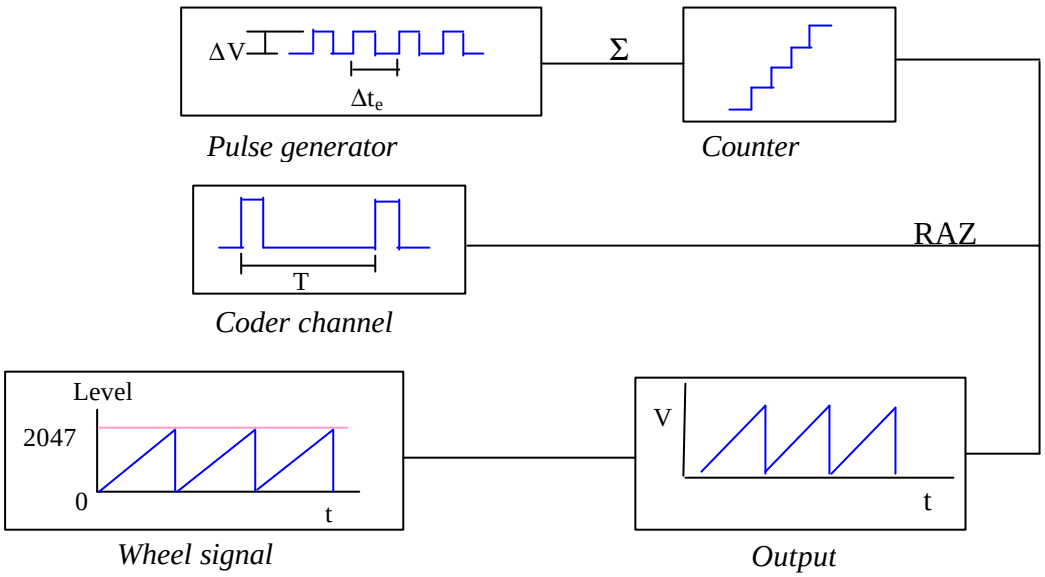

Figure 5: Coding system (where $\Delta t_e = 1/ f_e$, f_e is the pulse generator frequency and ΔV the pulse height).

These two variables (f_e , ΔV) are adjusted for each acquisition in order to obtain the best dynamic. In these conditions, the wheel angle is coded by an integer (called “input”, lesser than 2047) and registered on the velocity fields during the PIV measurements. Figure 6 shows an example of the “input” values during a PIV measurement.

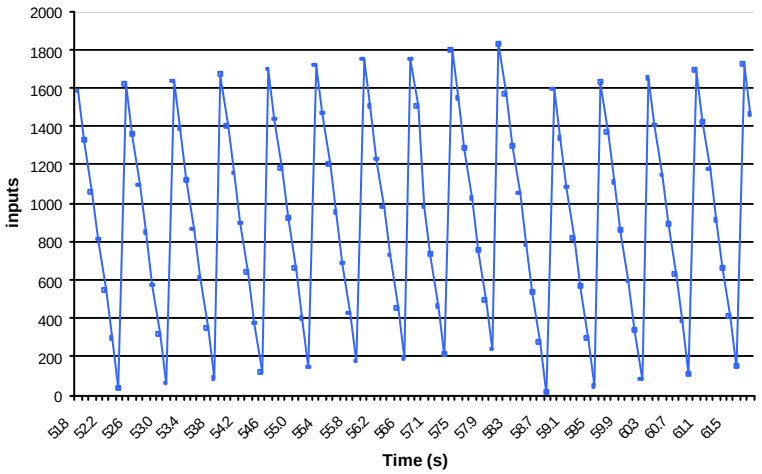

Figure 6: “Input” values according time.

During the set-up, we have observed several irregularities on the signals (time shift, electronic inertia, …). We have to detect and correct these problems with a software. At the end, we obtain the wheel angle from the following formula:

$$a=360*(Input/I_{max})$$

where *Input* is the corrected level and I_{max} le higher level obtained (corresponding to 360°).

Accuracy and bias : For most of the measurements, I_{max}=1800, in these conditions a level corresponds to 0.2°. But the power lathe does not have a constant rotating frequency. Thus, I_{max} is not constant turn to turn. It is also impossible to get this value for each turn because of the low frequency (10 Hz) of the PIV system. So, we have to estimate this value and we obtain an uncertainty on I_{max} about ±10 levels creating a systematic error ≈±0.55%.

Particle image velocimetry (PIV) was used to measure the velocity fields. The seeding of the flow was done by using a smoke generator that releases particles (solution of water and glycerin) having a diameter range between 1 to 10 µm. A pulsed laser (Nd-Yag Spectra-Physics 2x200 mJ) was used to illuminate the flow and to create a thin (≈1.5 mm) light sheet. A correlation CCD camera having a resolution of 768 x 484 pixels captured the images. The laser and the camera are connected to the synchronizing box of the Dantec FlowMap PIV 2000 processor. The PIV processor is connected to the computer and is controlled by the data acquisition program. The velocity fields were obtained and recorded on a computer while the Flow Manager v3.0 program controlled the whole acquisition process.

The treatment of data obtained experimentally was carried out in two phases. In fact, to render the velocity fields exploitable, a calibration (using a scale factor within the Flow Manager program) is made beforehand in order to express the velocity fields in m/s instead of pixels/s. Secondly, validation steps are carried out in order to eliminate erroneous velocity vectors using a Dantec software and a homemade software based on a global bandwidth filter.

The uncertainty analysis was performed for the measurement values by using a 95% confidence level. So measurement precision has been estimated to be less than 1%, and the maximum bias at 3% for the mean values and at 6% for the RMS values. These include the accuracy, the statistical bias and the position uncertainty.

A comparison between the phase (angular) average flow fields of several configurations allows us to analyze the influence of the main parameters of this study. Several planes (inside and outside the wheel) are studied (cf. figure 7). Three outside horizontal planes (E1, E2 and E3) to observe the flow field near the holes and two inside horizontal planes (I1 et I2) to study the flow in the vicinity of the brake disk.

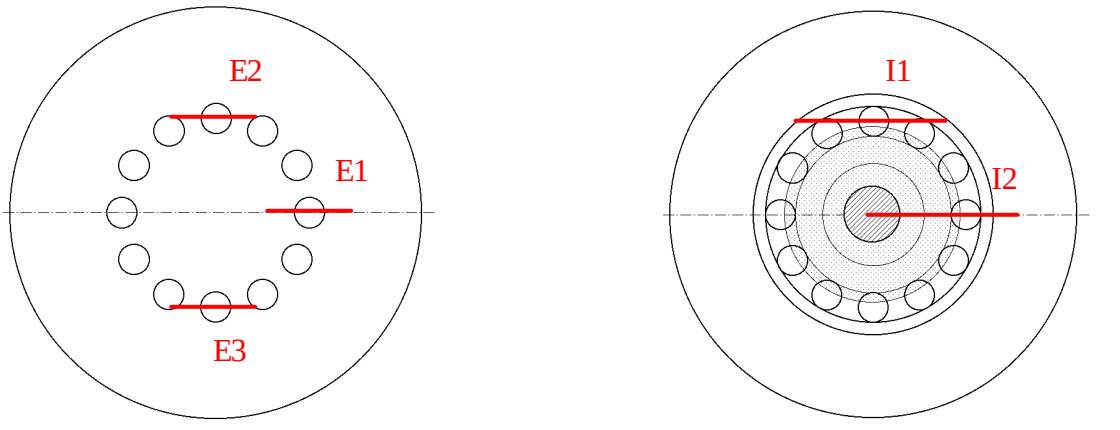

Figure 7: Outside and Inside planes of measurement.

Results and discussion

This paper presents the flow structure in the vicinity of a wheel model. In the first part we will describe the flow around the wheel and in a second part we will study the role of the interfaces (inside/outside) of the wheel.

Even if, in our case, the floor is steady, we observe the same flow behavior as that observed by Fackrell and Harvey (1973) for a wheel on a moving floor (cf. Figure 8): The arriving flow separates in front of the wheel

in order to bypass this obstacle. This separation occurs both in the vertical direction and the horizontal direction. In the vertical symmetry plan of the wheel, a separation line delimits two parts of the flow. The first one (located near the floor) goes toward the floor in accordance with the wheel rotation. The second part goes upward and follows the border of the wheel even if the rotation of the wheel is in a contrary direction. Figure 9 is obtained from a picture issuing from the LASER sheet visualizations realized in the horizontal symmetry plan (Y=0) of the wheel. It shows the separation line which divides the incoming flow in two parts: The first toward the wheel axle side and the second toward the side holes. We can observe that this separation seems to be symmetric and the same behavior is also observed near the floor by the wall streamlines obtained with the spreading over visualizations method.

Several separations have been observed on the flanks of the wheel: One on each side and a third one occurs on the top of the wheel where the incoming flow decelerates in the vicinity of the top of the wheel, because of the flow induced by the rotation of the wheel, and creates a separation (cf. reference).

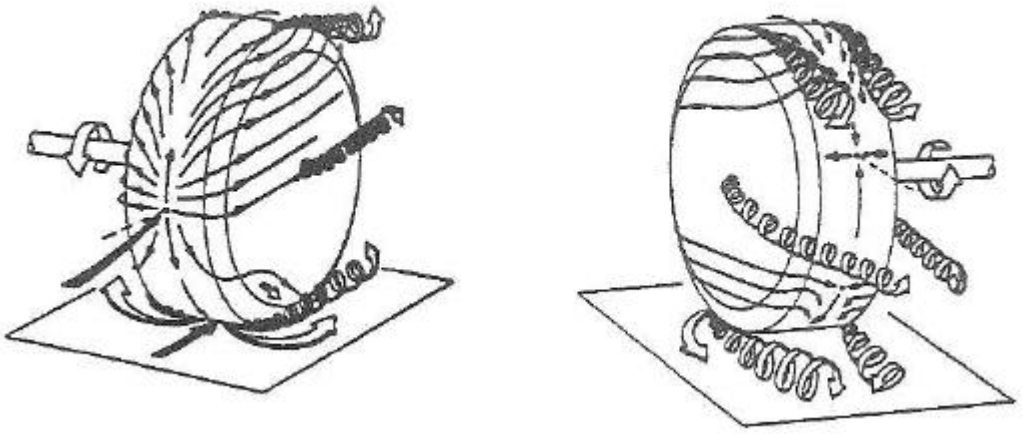

Figure 8: Flow around a rotating wheel on a moving floor (from Fackrell and Harvey (1973)).

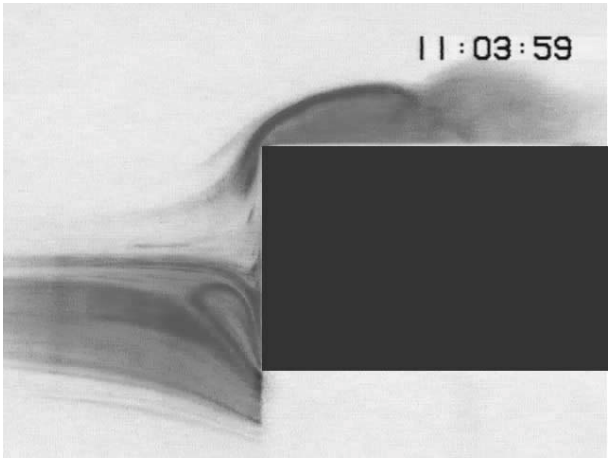

Figure 9: LASER sheet visualizations upstream the wheel (plan Y=0, top view).

A reverse flow area, induced by the separation of the main flow at the leading edge of the wheel (cf. figure 10), occupies a third of the wheel on both flank of the wheel (axle side & side holes). These results are deduced from the velocity field obtained by PIV, at 5 mm from de wheel. On figure 11, we have drawn the negative longitudinal component V_x in order to highlight the reverse flow area located on this side of the wheel. This area follows the curvature of the wheel and occupies most of the upstream part of the wheel on an angular sector included between ± 55°.

We also observe on figure 10 that the flow coming from upstream accelerates and bypasses the edge of the wheel. This creates a reverse flow area where the velocity is weaker. We can also note that this area is perturbed by the exit of the inner flow near the interface “inner/inner boundary”.

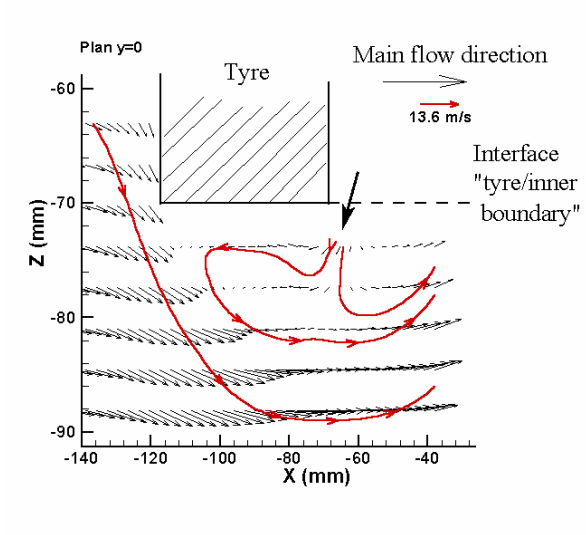

Figure 10: Velocity field in the plan Y=0

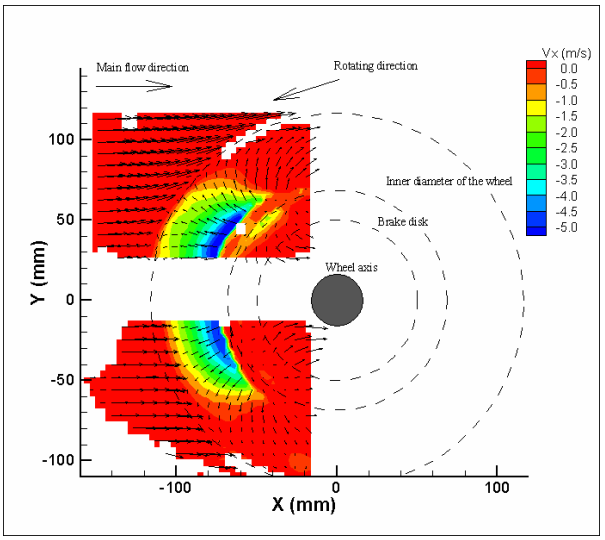

Figure 11: Velocity field in the plan Z=-75 mm.

On the axis side, the PIV measurements, in good agreement with those obtained for by LDA, indicate that the external flow enters through most of the interface (Inside/Outside). The velocity is very high upstream and upside the axle (The values reach 12 m/s for an external main flow of 13.6 m/s). On the other hand, the outward areas (V_z<0) are located in the upstream part of the interface "inside/outside" and in the axis wake. For this first location, the outflow is located in a crown between the radius 55 mm and the radius 68.5 mm (this last radius corresponds to the lower radius of the tire). The existence of this flow exit with low velocities (between 1 and 2 m/s) near the wheel is due to the reverse flow area (cf. figure 10). In this plan (Y=0), the exiting flow partly goes downstream and is partly aspired upstream because of the presence of a reverse flow zone upstream of the tire. For the second location (axis wake), the magnitude of the velocity is higher and we can observe velocities up to 9 m/s. Most of the flow exits off the wheel at this place because of the suction created by the area of low pressure reigning in the wake of the wheel axle.

Figure 12 is an image resulting from visualizations by LASER tomography carried out in a vertical plane passing by the center of the downstream holes position (X=53 mm). To carry out this visualization, only the inside part of the rotating wheel was sown. Thus, the spots of smoke, present on the image, reveal a flow exit by the holes when the wheel is not rotating. This behavior is confirmed and quantified with the transverse velocity component obtained by ADL in the center and between each opening of the wheel, with and without rotation. We observed that the transverse velocity component is, in general, positive in the center of the holes and negative between the holes. The highest speeds are reached in the centers of the holes upstream (the maximum transverse velocity (4.2 m/s)). From these observations, we can deduce that the flow leaves the majority of the wheel holes, except for the two holes located upwards. The negative values of V_z, apart from the holes, can be explained by the reattachment of the separation line present on the openwork side of the wheel.

Figure 12: Flow visualization in the plan X=53 mm.

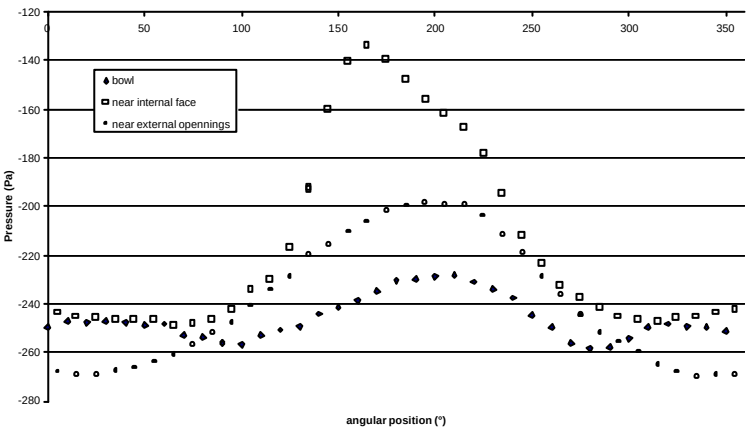

Figure 13: Angular pressure distribution

Figure 13 presents static pressure measurements obtained without rotation for the three taps located in the vicinity of an opening. Pressure is represented according to the angular position to which measurements were taken. The static pressure of the Pitot tube present at the entrance of the wind tunnel was subtracted from the pressures. We observe that the curves have a Gaussian shape and that the pressures are lowest when the taps are in the upstream part (angles included between 0° and 90° and between 270° and 360°). Moreover, the internal pressure is higher than the external pressure whatever the position of the taps. There is thus a negative pressure gradient between the inside and outside of the wheel which is responsible for the fluid exiting by the holes.

Figure 14 shows the average velocity field for the configuration without rotation in the horizontal plane including the downstream opening. According to the separation at the leading edge of the wheel, the velocities are always higher (around 17 m/s) than the main flow velocity at the entrance of the test section (13,5 m/s). In this configuration (without rotation), the opening is always located between the abscissas x=0 and x=17 mm. We observed a clear fluid exit on this interval characterized by high transverse velocities (V=5 m/s) and horizontal velocity fluctuations around 4.5 m/s. This exit also occurs in the second part of the holes (8≤x≤17 mm). The high RMS values (higher in the X-direction than the Z-direction) in this area are induced by the shear caused by the fluid exit.

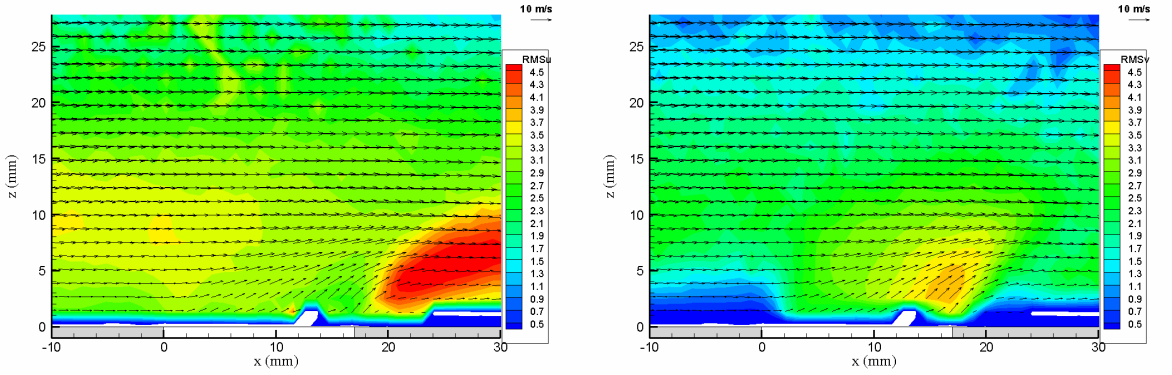

Figure 14: Velocity field, RMSu & RMSv - Plane E1 - Configuration D (without rotation).

Figure 15a shows the average velocity field for configuration F (i.e. Configuration D with rotation) but without taking into account the location of the opening during the acquisition. In these conditions, the results indicate that the average value of the transverse velocity component is weak (no flow through the holes) but we can observe quite high RMS values along the wheel. This can be explained by the fact that, at the measurement points, the fluid is seen coming out ($V_z>0$) and also impinging the wheel ($V_z<0$). On the other hand, for the configuration G (axisymmetric open wheel with rotation) we observe on the velocity field a weak fluid exit characterized by few vectors directed towards the outside and high RMSu values in the same area.

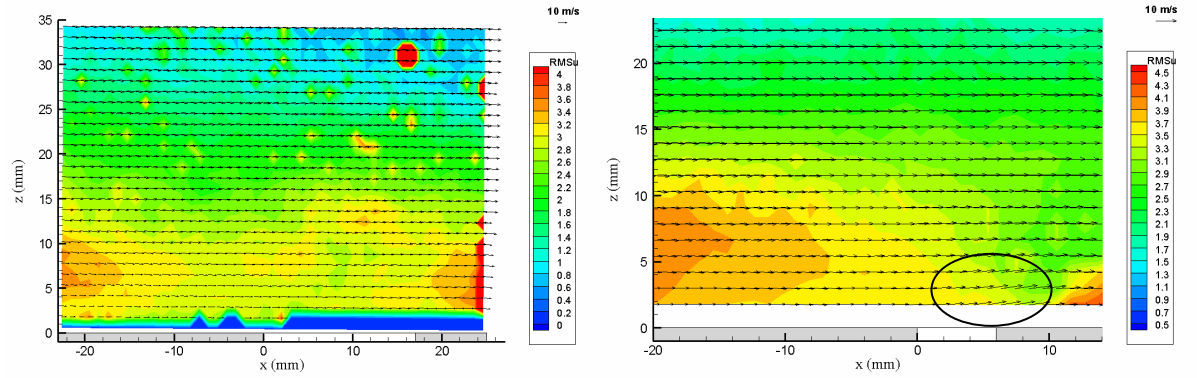

a) Configuration F b) Configuration G

Fig. 15: Average velocity field and RMSu (with rotation) – all angles -

For the outside plane E1, we have clearly observed a fluid exit when the wheel does not rotate (or for the axisymmetric case) but it seems that the rotation masks the fluid exit through the holes because of the velocity

average. For the other outside planes (E2 and E3), the flow fields are quite different. For configuration D the fluid enters inside the wheel through the upper hole (plane E2, figure 16a) while for the last plane, the flow exits the wheel on the second half part (8≤x≤17 mm) of the lower hole (E3, figure 16b) as previously observed for the first plane E1. Upstream of the holes, we observe a reverse flow area (always present whatever the configuration) due to the impact of the flow which separates slightly earlier at the leading edge of the wheel.

According the analysis of the others configurations, the results show that the main flow velocity (Ue), the rotating velocity (w) and the surface of the holes are limiting factors for the exchanges trough the holes: the more these parameters are weak, the more the exchanges are weak.

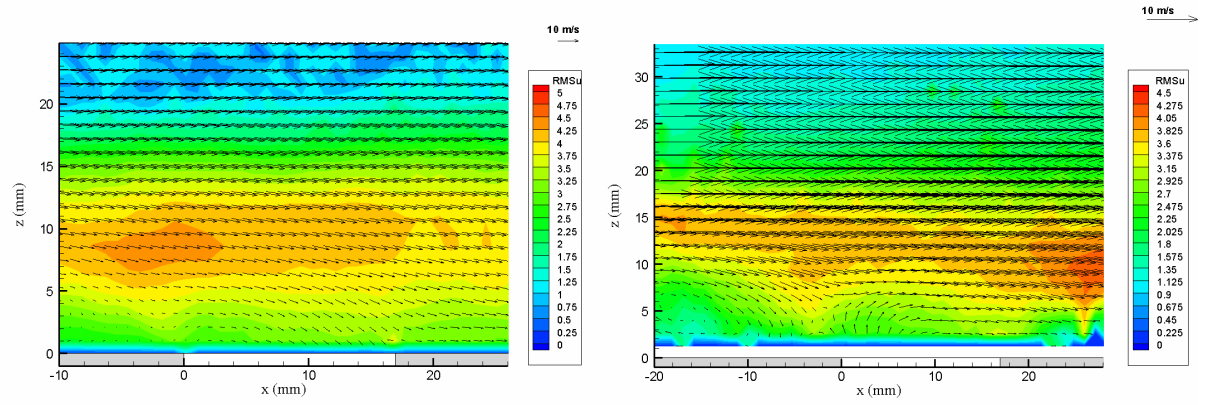

a) Plan E2 b) Plan E3

Figure16: Average velocity field and RMSu (without rotation) - Configuration D

It was more difficult to obtain accurate measurements inside the wheel because of the clogging and the reflections on the transparent walls. For configuration D (without rotation), we observe in plane I1 that the flow passes behind the brake disk before exiting by the holes (cf. figure 17a). Downstream (plan I2) the velocity field shows clearly a outward motion of the fluid which interacts with the main flow creating high level of unsteadiness (High RMSu values at x=40mm; z=-35mm) while another part follows the wheel axle (x=10mm; z=-35mm). A little part of the flow skirts and then bypasses the brake dis k (x=40mm ; z=0) participating to the "feeding" of the "bowl" before exhausting through the holes.

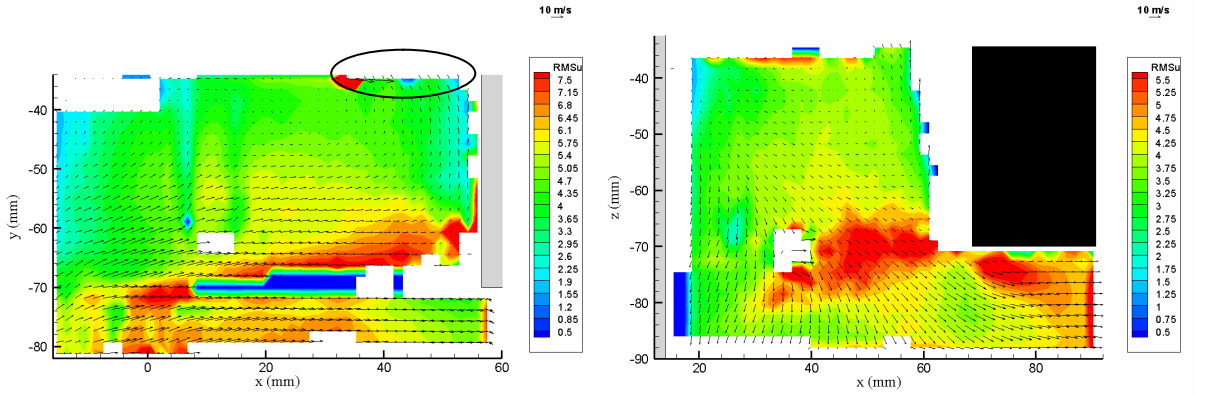

Plane I1 Plane I2

Figure 17: Average velocity field and RMSu (without rotation) - Configuration D.

One of the main interests of this study is to take into account the location of the holes and to average the velocity fields only when the angular positions of the wheel are the same. Considering the symmetry of the wheel, we have defined 30 classes (one for each degree). The value 0 and 30 corresponds to the configuration when the laser sheet impacts the wheel between two consecutive holes and the value 16 when the laser sheet impacts the middle of an opening. So, it is possible to process phase (angular) average velocity fields which is more representative of the dynamic of the flow.

Figure 18a shows the case where the laser sheet is located between the openings. In these conditions, the wall is continuous and we don't observe any flow through the wheel. On the other hand, figure 18b clearly indicates a flow exhausting from the wheel. For this configuration, the measurements are obtained when the

LASER sheet intersects the opening diameter where we observe velocity magnitude higher than for configuration G. Several movies have been built in order to analyze the unsteadiness of the flow. For configuration F, we clearly observe a periodic fluid exhausting by the downstream hole (plane E1) and a periodic inward motion for the planes E2 while the last outside plane (E3) reveals both. All these results have been compared (and completed) by hot wire measurements and are in good agreement with this other technique.

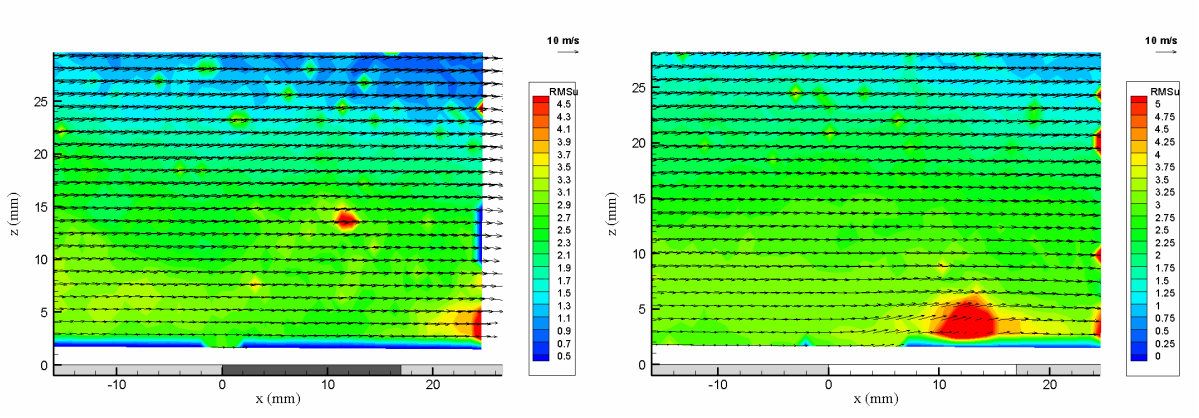

α= 0° α=15°

Fig. 18: Average velocity field and RMSu – Configuration F (with rotation)

Conclusion and perspectives

In conclusion, measurements were carried out by LDA, hot wire and PIV in the vicinity of a car wheel model. For several plans when the wheel is in rotation we have used "conditional" PIV measurements with the registration of the wheel position during the acquisition. Phase averages are then carried out. The processing of these measurements allowed us to observe a periodic fluid expulsion when a hole crosses the plan of measurement, revealing that the fluid comes out of the wheel trough most of the wheel holes.

However, the exit fluid velocities are usually lower and the disturbance of the separation area is less because of the distribution effect of the outgoing fluid by the holes. This distribution causes a local exit velocity fall.

The estimation of the flow rates passing through the holes show notable differences between the different configurations but they have to be improved using a time resolved PIV system before coupling to the heat transfer analysis.

References

Axon L; Garry K; Howell J (1998) An evaluation of CFD for modeling the flow around stationary and rotating isolated wheels. SAE paper 980032, 65-75.

Cogotti A (1983) Aerodynamic characteristics of car wheels - Impacts of aerodynamics on vehicle design. International Journal of Vehicle Design, SP3, 173-196.

Cogotti A (1991) Wake Survey of an Isolated Wheel. Preliminary Report of Pininfarina Industry. Ref. N°. 3190.

Fackrell JE; Harvey JK (1973) The flow field and pressure distribution of an isolated road wheel. BHRA «Advances in road vehicle aerodynamics», Paper 10.

Fackrell JE; Harvey JK (1974) The aerodynamics of an isolated road wheel. AIAA 2nd Symposium, «Aerodynamic and racing cars», vol. 16, AIAA lecture series.

Mercker E; Breuer N; Berneburg H; Emmelman HJ (1991) On the aerodynamic interference due to the rolling wheels of passengers cars. SAE technical paper 910311.

Mercker E; Berneburg H (1992) On the simulation of road driving of a passenger car in a wind tunnel using a moving belt and rotating wheels. Congresso ATA «Innovation and reliability in automotive design and testing», Firenze (ITALY).

Noel A (2001) Etude expérimentale des phénomènes aérothermiques liés aux disques de freins automobiles. PhD Thesis, Université de Poitiers, FRANCE.

Stapelford WR; Carr GW (1970) Aerodynamic characteristics of exposed rotating wheels. MIRA Report 1970/2.